Geophysical Research Letters

RESEARCH LETTER
10.1029/2018GL081168

Key Points:
- Double seismic zone geometrical structure is controlled by plate age and the slab's thermal parameter
- We find consistently larger *b* values for the upper seismicity layer, correlating with slab age, and roughly constant values for the lower
- Our results are consistent with dehydration embrittlement operating in the upper layer but point to a relatively dry lithospheric mantle

Supporting Information:
- Supporting Information S1

Correspondence to:
M. A. Florez,
mflorez@mit.edu

Citation:
Florez, M. A., & Prieto, G. A. (2019). Controlling factors of seismicity and geometry in double seismic zones. *Geophysical Research Letters*, *46*. https://doi.org/10.1029/2018GL081168

Received 31 OCT 2018
Accepted 12 MAR 2019
Accepted article online 10 APR 2019

Controlling Factors of Seismicity and Geometry in Double Seismic Zones

M. A. Florez[1] **and G. A. Prieto**[2]

[1]Department of Earth, Atmospheric, and Planetary Sciences, Massachusetts Institute of Technology, Cambridge, MA, USA, [2]Departamento de Geociencias, Universidad Nacional de Colombia-Sede Bogotá, Bogota, Colombia

Abstract Double seismic zones are ubiquitous features of subduction zones, where seismicity is distributed along two layers separated by a region with significantly less seismic activity. Dehydration embrittlement is thought to be responsible for earthquakes in the subducting crust (upper layer), but the case for it in the lithospheric mantle (lower layer) is less clear. We apply a recently developed relative relocation technique to characterize seismicity in 32 slab segments. The high-precision hypocentral depths allow us to assign events to either the upper or lower layer and to separately estimate frequency size distributions for each plane. We find consistently larger *b* values, correlating with slab age, for the upper layer and roughly constant values for the lower. We also show that thermal parameter and plate age are the key controls on double seismic zone geometry. Our results point to a relatively dry lower layer and suggest a fundamentally different mechanism for lithospheric mantle earthquakes.

Plain Language Summary Despite being a common feature of global seismicity, intermediate-depth earthquakes (70–350 km in depth approximately) and their physical mechanism are not well understood. These earthquakes occur at pressures and temperatures incompatible with our current models of brittle failure. At those depths, most subducting slabs feature two separate layers of seismicity, with little activity in-between. It is commonly believed that the release of high-pressure fluids enables the brittle-like behavior; however, it is not yet clear whether this mechanism can operate on both layers. We have applied a recently developed earthquake location technique to construct a new global catalog of intermediate-depth seismicity. We use this data set to study the geometrical structure of the two layers and their statistical characteristics. Our results point to a relatively dry lithospheric mantle—lower layer—regardless of plate age, convergence velocity, or composition and suggest that the physical mechanism enabling rupture in the lower layer is fundamentally different from the one in the upper.

1. Introduction

Double seismic zones (DSZs) are a common feature of seismicity in subducting slabs (Brudzinski et al., 2007). Multiple studies have shown that earthquakes within the subducting lithosphere cluster into two distinct layers (Hasegawa et al., 1978; Hasegawa & Nakajima, 2017; McGuire & Wiens, 1995; Rietbrock & Waldhauser, 2004) that eventually merge at depth (Green et al., 2010; Wei et al., 2017). The region between the two has little or no seismicity, and their average separation correlates with plate age (Brudzinski et al., 2007). Earthquakes located in the upper seismicity layer (USL) are inferred to occur within the subducting oceanic crust and/or uppermost mantle, while the lower seismicity layer (LSL) appears to occur in the subducting lithospheric mantle (Green et al., 2010; Peacock, 2001; Wei et al., 2017). Seismicity in the USL is generally believed to be due to fluid overpressure linked to dehydration reactions within the crust or uppermost mantle (Hacker et al., 2003; Kirby, 1995; Okazaki & Hirth, 2016). In contrast, the mechanism for seismicity in the LSL is much more controversial (Ferrand et al., 2017; Ohuchi et al., 2017; Peacock, 2001; Reynard et al., 2010). Recent work in the laboratory and field observations suggest that faulting at intermediate depths may occur under dry conditions (Ohuchi et al., 2017; Scambelluri et al., 2017), although it was recently shown that a partially hydrated lithospheric mantle could produce failure by a stress transfer mechanism driven by dehydration reactions in a partially hydrated uppermost mantle (Ferrand et al., 2017; Kita & Ferrand, 2018; Scambelluri et al., 2017).

A possible pathway for water to infiltrate into the subducting mantle is through faulting and plate bending at the trench (Faccenda et al., 2009, 2012; Korenaga, 2017; Ranero et al., 2003), although how deep can water go

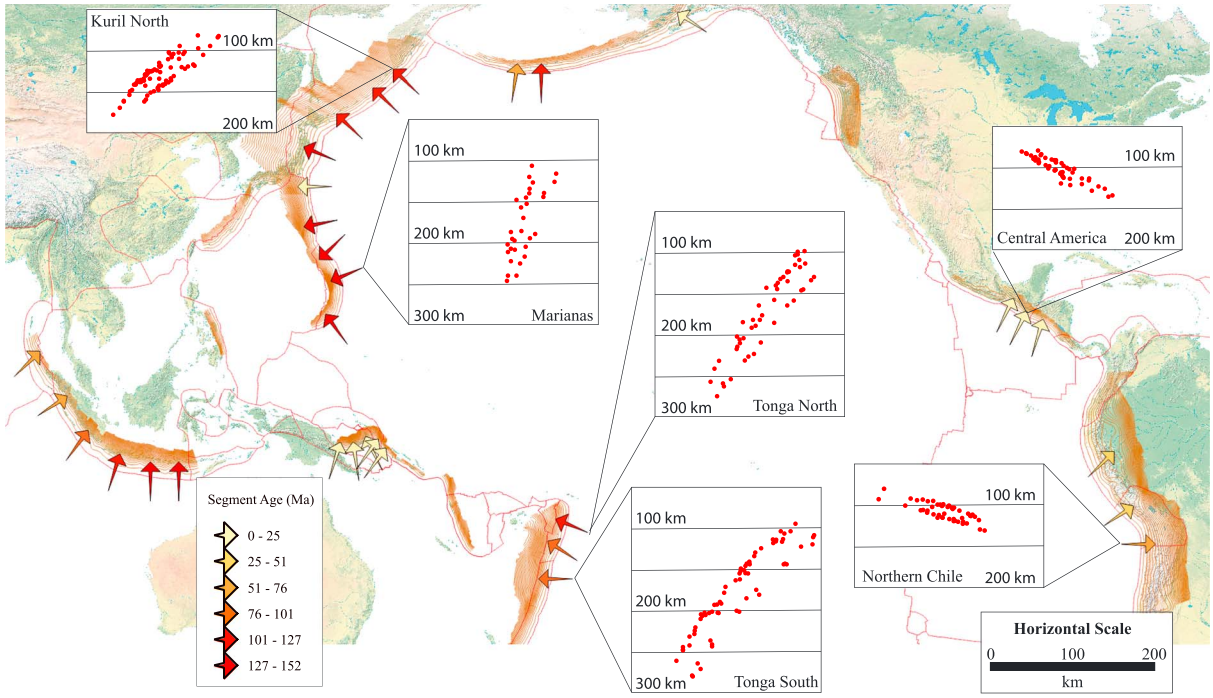

Figure 1. Global map view of major subduction zones with depth contours (orange lines) that follow the Slab1.0 model (Hayes et al., 2012). Arrows represent the segments analyzed, point in the direction of relative plate motion, and are color coded by age. Vertical cross sections display the improved locations (red dots) and are drawn at the same scale. At each segment analyzed a DSZ was observed, making this pattern of seismicity a global feature as first proposed by Brudzinski et al. (2007).

and how pervasive this mechanism could be, remain controversial (Korenaga, 2017; Syracuse et al., 2008). Reduced *Vp* anomalies are often found along the LSL (Dorbath et al., 2008); in some cases, the high *Vp/Vs* ratios expected for a highly serpentinized mantle or fluid saturated rock are not observed (Dorbath et al., 2008; Syracuse et al., 2008), while other results point towards a hydrated lithospheric mantle (Bloch et al., 2018; Cai et al., 2018). Anisotropy of anhydrous peridotite may provide a better explanation for the inferred seismic velocity anomalies (Hasegawa & Nakajima, 2017; Ranero et al., 2003), imposing an additional constraint on the triggering mechanism: it must also operate under relatively dry conditions. Therefore, brittle-like failure driven by a thermal shear instability is also viable and potentially more likely (John et al., 2009; Kelemen & Hirth, 2007; Ohuchi et al., 2017) for earthquakes in the LSL.

The presence (or absence) of fluids (among other factors) is known to affect the relative number of small to large earthquakes in subduction zones (Katsumata, 2006; Kita & Ferrand, 2018; Wiemer & Benoit, 1996; Wyss et al., 2001), that is, the *b* value in the frequency size distribution of seismicity; a small *b* value implies a relatively large number of big events. In Alaska, New Zealand, Japan, and the Lesser Antilles high *b* value anomalies take the shape of a bull's-eye, at the top of the slab, and correlate with regions where dehydration reactions are expected (Katsumata, 2006; Wiemer & Benoit, 1996). Also, *b* value measurements have become proxies for the presence of fluids under volcanic arcs (van Stiphout et al., 2009; Wyss et al., 2001). Accurate locations combined with careful statistical analysis offer the unique opportunity of assessing the relative abundance of fluids and the triggering mechanism of earthquakes in DSZ worldwide.

We systematically apply the relocation method proposed by Florez and Prieto (2017) to generate a new global catalog of intermediate-depth seismicity. This data set enables us to study 32 slab segments that sample a broad range of subducting slab physical conditions, plate ages, convergence velocities, and thermal parameters (e.g., Weins, 2001), determined from the slab's age, convergence velocity, and dip angle (Figure 1). We investigate the relationship between width and depth extent of DSZs and the physical properties of the subducting slab and analyze the statistical behavior of seismicity in the USL and the LSL in terms of both productivity and frequency size distribution.

2. Earthquake Relocation Using Depth Phases

The width of a DSZ varies from a few to about 40 km (Brudzinski et al., 2007). When compared with this length scale typical location errors in global seismicity catalogs can be significant. Hypocentral depth is particularly problematic most event locations in global catalog have well constrained epicenter, due to good azimuthal coverage, but lack vertical resolution (Engdahl et al., 1998). The main sources of error affecting the accuracy of global seismicity catalogs are (i) random phase picking errors (Richards-Dinger & Shearer, 2000; Shearer, 1997); (ii) systematic biases introduced by using an average 1-D velocity model (Lin & Shearer, 2005; Waldhauser & Ellsworth, 2000); this is especially important in subduction zones where lateral velocity variations can be as large as 10% of the background model (Engdahl et al., 1998); and (iii) insufficient use of phases whose raypaths have good vertical coverage (Engdahl et al., 1998). Depth errors of about 40 km are not uncommon.

To overcome these limitations, we use the algorithm developed by Florez and Prieto (2017), first applied to resolve a well-known DSZ in Northern Chile with only data from permanent arrays in the western United States. We take advantage of array processing techniques to automatically measure *pP-P* differential arrival times and then combine these measurements into a relative relocation scheme to reduce velocity model biases (Florez & Prieto, 2017). We relocate clusters of 50 to 150 neighboring earthquakes at a time. The set of best fitting relative depths is obtained using the AK135 (Kennett & Engdahl, 1991) global 1-D average velocity model. Initial hypocenters are extracted from the reviewed International Seismological Centre catalog (International Seismological Centre, 2015). Typical relative depth errors are of the order of 1 to 2 km.

We apply this technique worldwide. We chose narrow and smooth plate segments with as many large intermediate-depth earthquakes as possible (Brudzinski et al., 2007; Nishikawa & Ide, 2014; Syracuse et al., 2010). We sample every major subduction zone and the entire range of plate ages, from 10 to 150 Ma (Data S1 in the supporting information). We avoid triple junctions and zones of highly oblique plate motion. Array processing techniques work effectively when applied to a large number of closely spaced stations; these arrays must be at specific distances from the events to avoid triplications that contaminate the arrivals of interest; *pP* is cleanly observed at 30° or more and *sP* is detected between 16° and 19°. Consistency is also important (Florez & Prieto, 2017); we use dense regional networks that have been in operation since at least 2000, mainly in Japan, the western United States, Australia, New Zealand, and Taiwan. These criteria limit the number of segments we can study; however, careful data selection allows us to analyze 32 slab segments; see Table S3 for a description of the parameters that define them. Each segment analyzed shows a clear DSZ, significant variations in width and depth extent are readily observed (Figure 1). In regions such as Vanuatu, Ryukyu, Philippines, and the Caribbean, we were unable to assess the presence of a DSZ; data at the required distance range was not available at the time of this study.

3. DSZ Characterization

Earlier work by Brudzinski et al. (2007) used global catalogs to statistically assess the presence of a DSZ. By taking small segments and rotating their seismicity in the slab downdip direction, it is possible to test if the obtained pattern can be fit by a bimodal Gaussian distribution; if so, the width of the DSZ is simply estimated as the distance between the Gaussian peaks. Nevertheless, this idea only allows to assert the presence of a DSZ detailed characterization of its geometry and seismicity has relied on local networks located on top of a few slab segments (Kita et al., 2010; Rietbrock & Waldhauser, 2004).

Our new catalog has sufficient resolution to systematically explore the factors that control DSZ geometry and to separate seismicity into earthquakes belonging to either the upper layer or the lower. We use a smoothing splines interpolation to determine the optimal USL and LSL, assigning earthquakes to one of the layers depending on their closeness to each splines curve (Figure 2). The interpolation is performed iteratively. We calculate a starting DSZ width using a bimodal Gaussian fit (Brudzinski et al., 2007). Based on this initial width and the location of the two peaks an initial assignment of events is made to either the USL or the LSL. Then, the two layers of seismicity are fitted separately using a smoothing spline interpolation. The procedure is performed iteratively until the following two criteria are satisfied: (i) the splines intersect each other at a depth which is within 30 km of the deepest earthquake found in the segment and (ii) the width, measured as the average distance between the two splines (only for the first three fourths of the dipping slab segment), is within 20% of the initially estimated width. Events are also iteratively assigned to either the USL or the LSL.

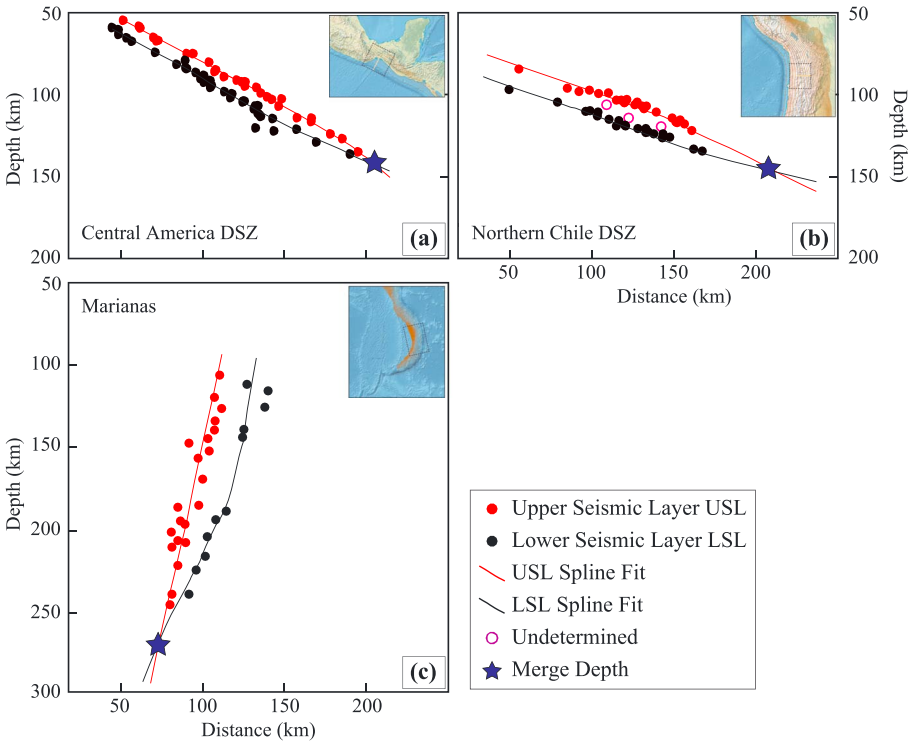

Figure 2. Estimation of double seismic zone (DSZ) width and maximum depth extent (star) and separation of USL and LSL seismicity (red and black circles) for three segments. (a) For the relocated catalog in northern Chile, a smoothing spline is used for fitting the upper and lower seismicity (red and black lines respectively). The maximum DSZ depth or merging depth is defined at the merging point of the two spline curves, and the DSZ width is based on the separation between the upper and lower spline curves. For each slab segment, seismicity is separated in USL and LSL according to the distance to either the upper or lower spline curves. In the case where an earthquake is at a similar distance to either spline, it is undetermined whether it belongs to the USL or LSL (empty circle). (b) Similar to (a), for the Central America DSZ. (c) Similar to (a) for the Japan DSZ. (d) Similar to (a) for the Marianas DSZ. USL = upper seismicity layer; LSL = lower seismicity layer.

For every event, the smallest distance to each of the two spline curves is determined. If the two distances are within 10% of each other, the event is not assigned to any particular layer; otherwise, it is assigned to the layer corresponding to the nearest curve. If after 20 iterations the above mentioned criteria are not satisfied, the width of the DSZ is set to the initially determined one and no depth extent measurement is performed for that segment.

We analyze DSZ geometry in terms of two variables: depth extent and width. The depth extent corresponds to the depth at which the two splines curves intersect. To determine the width of the DSZ, we estimate the average distance between them in the slab-normal direction (Brudzinski et al., 2007); since the curves typically merge at depth, the width is only estimated using the first 75% of the points in the down-dip direction, to avoid underestimating the width due to the closure of the DSZ. Our results on the width are compared to a bimodal Gaussian fit of seismicity (Brudzinski et al., 2007; Syracuse et al., 2008) with excellent agreement.

Our relocated catalog provides robust evidence of the ubiquity of DSZ and the strong correlation of DSZ width and plate age (Figure 3), in agreement with previous work (Brudzinski et al., 2007). Indeed, variables such as thermal parameter (Figure 3), arc-trench distance, and convergence velocity poorly correlate with DSZ width (Figure S1). This is sometimes explained by the depth of hydration of the incoming slab, which is limited by the slab temperature and the stability of hydrated phases (Ranero et al., 2003). In contrast, the depth extent is mostly controlled by the thermal parameter (Figure S2). The latter result is similar to that presented for Tonga, and other subduction zones (Wei et al., 2017), estimated by visual inspection of DSZs reported in the literature and suggests that temperature must play a role in any viable mechanism for intermediate depth earthquakes.

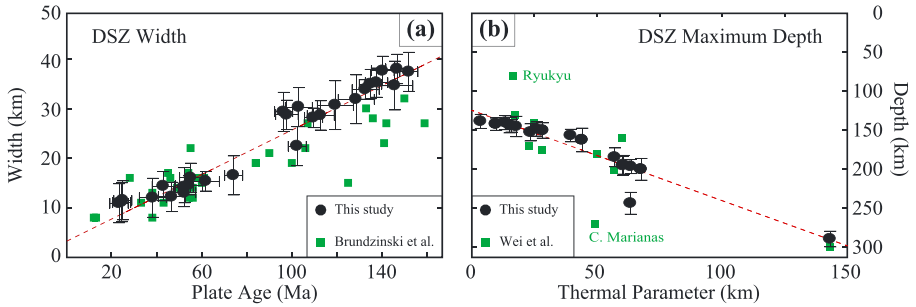

Figure 3. Observed dependence of double seismic zone (DSZ) characteristics and plate properties at global scales. (a) DSZ width is correlated with plate age, similar to previous (green squares) results (Brudzinski et al., 2007), although our estimated values are larger for older plates, which could be explained by the different width determination methods. Our method does not use the earthquakes that are deeper in the region where the USL and LSL merge. (b) The maximum depth of the DSZ (merging point of the USL and LSL) is heavily dependent of thermal properties of the subducting slab. Compiled results (green squares) from various subduction zones (Wei et al., 2017) show a similar behavior to our results. Outliers are marked for the compiled results. USL = upper seismicity layer; LSL = lower seismicity layer.

4. Frequency-Magnitude Statistics

Counting events may not be the most useful statistical characterization of seismicity the size of each earthquake also needs consideration. We estimate frequency-magnitude statistics independently for the USL and the LSL (Figure 4), for as many different regions as possible (see supporting informaiton and Figures S6 and

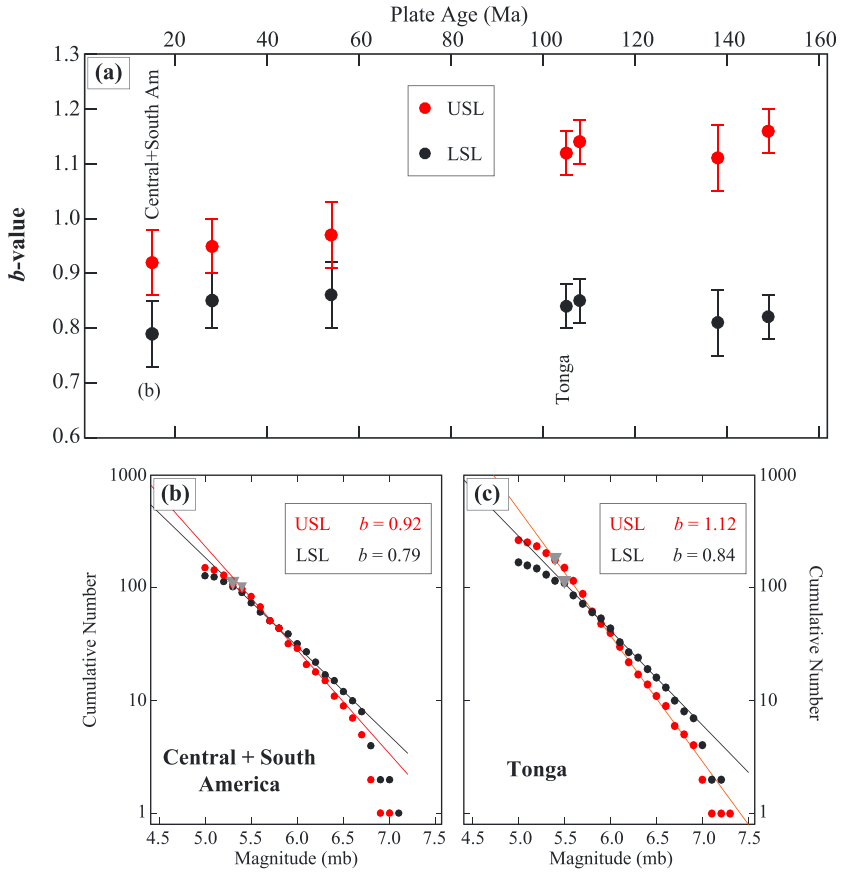

Figure 4. The *b* value differences between upper and lower double seismic zone layers. (a) Estimated *b* values and bootstrap errors for the USL and LSL as a function of plate age. In some cases, slab segments of similar age are combined to obtain a robust estimate. (b) Frequency-magnitude distribution for events in Central and South America, for the USL (red dots) and the LSL (black dots). Gray triangles represent Mc. Red and black lines represent the slope or *b* value estimated. (c) Same as (b) but for the Tonga slab segment. USL = upper seismicity layer; LSL = lower seismicity layer.

S7 for details concerning data selection and robustness of calculations). To obtain meaningful and robust statistics, we group nearby slab segments and separate events into two categories: those belonging to the USL and those belonging to the LSL. If the total number of events in each one of the two categories exceeds 100, we calculate both *b* values by applying a maximum likelihood method (Aki, 1965; Bender, 1983; Wiemer & Wyss, 2000). Our calculation uses the maximum curvature technique to estimate the completeness magnitude (*Mc*; Woessner & Wiemer, 2005). We obtain independent *b* value measurements for the USL and the LSL in as many different regions as possible (Figure 4). The age of each region is simply computed as the arithmetic average of the ages of the segments it contains.

We consistently find that the USL has significantly larger *b* values than the LSL. USL *b* values positively correlate with plate age, resembling the strong correlation between age and *b* value found for shallow subduction zone earthquakes (Nishikawa & Ide, 2014). In contrast, *b* values remain mostly constant for the LSL, with an average of about 0.8. Previous studies have found large *b* value anomalies near the top of some slab segments (Katsumata, 2006; van Stiphout et al., 2009; Wiemer & Benoit, 1996; Wyss et al., 2001); our results suggest that these differences are systematic, may be controlled by a few physical parameters, and are a global feature. Recent work in Japan (Kita & Ferrand, 2018) show larger *b* values in Hokkaido along the USL but have lower *b* values in the Tohoku area. Our results do not have the resolution to be able to compare each segment but point toward a global systematic behavior of *b* values between USL and LSL.

We are aware that the number of events used to estimate the *b* value for each region is small, although similar numbers have been used to study frequency size statistics (Nishikawa & Ide, 2014; Schorlemmer et al., 2005; Woessner & Wiemer, 2005; Prieto et al., 2012). We evaluated the robustness of the difference in *b* values between USL and LSL using a *t* test (Andrade & Estévez-Pérez, 2014; Pacheco et al., 1992; Blair & Higgins, 1980; Fay & Proschan, 2010) and can reject the hypothesis that the two *b* values are the same to the 0.998 confidence (see supporting information for a more complete explanation of the statistical tests). Figure S8 shows the global comparison of the frequency size statistics of USL and LSL seismicity, and their ratio, confirming that the *b* value difference is significant between the two layers.

5. Discussion and Conclusions

Our ability to clearly define DSZ geometry allows us to assign earthquakes to either the USL or the LSL with little ambiguity (Figure 2). A few scattered reports (Korenaga, 2017; Wei et al., 2017) suggest that seismicity rate—the number of earthquakes per year—is considerably smaller in the lower layer, as compared to the upper. Our results provide a partial explanation for this observation: the slab's thermal parameter exerts an important control on relative seismicity rates (Figure S3) colder subducting plates show higher rates for their USL, Tonga (Figure S4), arguably the coldest known slab, has a lower layer with a surprisingly small number of earthquakes (Wei et al., 2017). Warmer slabs display roughly equal rates for both planes (Figure S3). This issue deserves further investigation using local catalogs with smaller completeness magnitudes.

Previous studies have shown that high *b* values anomalies correlate well with regions where dehydration reactions are expected (Wiemer & Benoit, 1996; Wyss et al., 2001) or fracture zones where abundant fluids are present (Schlaphorst et al., 2016); therefore, *b* values along subduction zones provide an indirect assessment of fluid content. A relatively dry lithospheric mantle (lower layer) may explain the consistently smaller *b* values observed regardless of subducting plate age, thermal parameter, or composition. This has important implications for the mechanism of intermediate-depth earthquakes, thought to occur as the consequence of a series of dehydration reactions (Hacker et al., 2003; Kirby, 1995; Yamasaki & Seno, 2003).

Dehydration-induced fluid overpressure would be consistent with the higher *b* value observed in the USL but very unlikely to play a significant role in the triggering of lower layer seismicity (Chernak, 2011; Hilairet et al., 2007; Proctor & Hirth, 2015; Reynard et al., 2010; Zhang et al., 2004). Our results suggest a relatively dry lithospheric mantle hosting intermediate-depth earthquakes. This is in agreement with recent work in the laboratory and the field where failure is observed in dry rocks, within a partially hydrated mantle. Dehydration reactions in the minerals within the mantle trigger rupture in the dry rocks by transferring stresses due to volumetric changes (Ferrand et al., 2017; Kita & Ferrand, 2018; Scambelluri et al., 2017). This mechanism is known as a dehydration-driven stress transfer and does not require a highly hydrated lithospheric mantle. In fact, if the rocks are fully hydrated, the stress transfer mechanism is not efficient (Ferrand et al., 2017). However, other mechanisms that do not require highly hydrated rocks (e.g.,

thermal shear runaway) cannot be entirely ruled out. Further experimental, observational, and computational investigations are needed to understand the details of the process responsible for LSL earthquakes.

Whatever the actual mechanism might be the systematic *b* value differences reported here suggest that a fundamentally different process enables lithospheric mantle earthquakes.

Acknowledgments
We thank Victor Tsai, Marine Denolle, Satochi Ide, Matej Pec, Yusuke Mukuhira, Gavin P Hayes, our Editor, and Thomas P. Ferrand, one of our reviewers, for their helpful comments and suggestions. This work was partially supported by NSF grant EAR 1521534. Raw seismic waveforms were downloaded from the IRIS DMC (http://ds.iris.edu/ds/nodes/dmc/data/) and Japan's NIED (http://www.hinet.bosai.go.jp/about_data/). Catalogs containing starting earthquake hypocenters and magnitude information were obtained from the ISC (http://www.isc.ac.uk/iscbulletin/), all of which are public data repositories. The generated catalog with relocations is provided in the supporting information.

References

Aki, K. (1965). Maximum likelihood estimate of *b* in the formula log $n = a - bm$ and its confidence limits. *Bulletin. Earthquake Research Institute, University of Tokyo*, *43*, 237–239.

Andrade, J. M., & Estévez-Pérez, M. G. (2014). Statistical comparison of the slopes of two regression lines: A tutorial. *Analytica Chimica Acta*, *838*, 1–12. https://doi.org/10.1016/j.aca.2014.04.057

Bender, B. (1983). Maximum-likelihood estimation of *b*-values for magnitude grouped data. *Bulletin of the Seismological Society of America*, *73*, 831–851.

Blair, R. C., & Higgins, J. J. (1980). A comparison of the power of Wilcoxon's rank-sum statistic to that of student's t statistic under various nonnormal distributions. *Journal of Educational Statistics*, *5*(4), 309–335.

Bloch, W., John, T., Kummerow, J., Salazar, P., Krüger, O. S., & Shapiro, S. A. (2018). Watching dehydration: Seismic indication for transient fluid pathways in the oceanic mantle of the subducting Nazca slab. *Geochemistry, Geophysics, Geosystems*, *19*, 3189–3207. https://doi.org/10.1029/2018GC007703

Brudzinski, M. R., Thurber, C. H., Hacker, B. R., & Engdahl, E. R. (2007). Global prevalence of double Benioff zones. *Science*, *316*(5830), 1472–1474. https://doi.org/10.1126/science.1139204

Cai, C., Wiens, D. A., Shen, W., & Eimer, M. (2018). Water input into the Mariana subduction zone estimated from ocean-bottom seismic data. *Nature*, *563*, 389–392.

Chernak (2011). Syndeformational antigorite dehydration produces stable fault slip. *Geology*, *39*(9), 847–850. https://doi.org/10.1130/G31919.1

Dorbath, C., Gerbault, M., Carlier, G., & Guiraud, M. (2008). Double seismic zone of the Nazca plate in northern Chile: High-resolution velocity structure, petrological implications, and thermomechanical modeling. *Geochemistry, Geophysics, Geosystems*, *9*, Q07006. https://doi.org/10.1029/2008GC002020

Engdahl, E. R., van der Hilst, R., & Buland, R. (1998). Global teleseismic earthquake relocation with improved travel times and procedures for depth determination. *Bulletin of the Seismological Society of America*, *88*(3), 722–743.

Faccenda, M., Gerya, T. V., & Burlini, L. (2009). Deep slab hydration induced by bending-related variations in tectonic pressure. *Nature Geoscience*, *2*(11), 790–793.

Faccenda, M., Gerya, T. V., Mancktelow, N. S., & Moresi, L. (2012). Fluid flow during slab unbending and dehydration: Implications for intermediate-depth seismicity, slab weakening and deep water recycling. *Geochemistry, Geophysics, Geosystems*, *13*, Q01010. https://doi.org/10.1029/2011GC003860

Fay, M. P., & Proschan, M. A. (2010). Wilcoxon-Mann-Whitney or *t*-test? On assumptions for hypothesis tests and multiple interpretations of decision rules. *Statistics Surveys*, *4*(0), 1–39. https://doi.org/10.1214/09-SS051

Ferrand, T. P., Hilairet, N., Incel, S., Deldicque, D., Labrousse, L., Gasc, J., et al. (2017). Dehydration-driven stress transfer triggers intermediate-depth earthquakes. *Nature Communications*, *8*, 15247. https://doi.org/10.1038/ncomms15247

Florez, M. A., & Prieto, G. A. (2017). Precise relative earthquake depth determination using array processing techniques. *Journal of Geophysical Research: Solid Earth*, *122*, 4559–4571. https://doi.org/10.1002/2017JB014132

Green, H. W. 2nd, Chen, W. P., & Brudzinski, M. R. (2010). Seismic evidence of negligible water carried below 400-km depth in subducting lithosphere. *Nature*, *467*(7317), 828–831. https://www.ncbi.nlm.nih.gov/pubmed/20927105, https://doi.org/10.1038/nature09401

Hacker, B. R., Peacock, S. M., Abers, G. A., & Holloway, S. D. (2003). Subduction factory 2. Are intermediate-depth earthquakes in subducting slabs linked to metamorphic dehydration reactions? *Journal of Geophysical Research*, *108*(B1), 2030. https://doi.org/10.1029/2001JB001129

Hasegawa, A., & Nakajima, J. (2017). Seismic imaging of slab metamorphism and genesis of intermediate-depth intraslab earthquakes. *Progress in Earth and Planetary Science*, *4*. https://doi.org/10.1186/s40645-017-0126-9

Hasegawa, A., Umino, N., & Takagi, A. (1978). Double-planed structure of the deep seismic zone in the northeastern Japan arc. *Tectonophysics*, *47*(1-2), 43–58. http://www.sciencedirect.com/science/article/pii/0040195178901506, https://doi.org/10.1016/0040-1951(78)90150-6

Hayes, G. P., Wald, D. J., & Johnson, R. L. (2012). Slab1.0: A three-dimensional model of global subduction zone geometries. *Journal of Geophysical Research*, *117*, B01302. https://doi.org/10.1029/2011JB008524

Hilairet, N., Reynard, B., Wang, Y. B., Daniel, I., Merkel, S., Nishiyama, N., & Petitgirard, S. (2007). High-pressure creep of serpentine, interseismic deformation, and initiation of subduction. *Science*, *318*(5858), 1910–1913.

International Seismological Centre (2015). On-line bulletin. *Internatl. Seismol. Cent.*

John, T., Medvedev, S., Rupke, L. H., Andersen, T. B., Podladchikov, Y. Y., & Austrheim, H. (2009). Generation of intermediate-depth earthquakes by self localizing thermal runaway. *Nature Geoscience*, *2*, 137–140. https://doi.org/10.1038/NGEO419

Katsumata, K. (2006). Imaging the high b-value anomalies within the subducting Pacific plate in the Hokkaido corner. *Earth, Planets and Space*, *58*(12), E49–E52.

Kelemen, P. B., & Hirth, G. (2007). A periodic shear-heating mechanism for intermediate-depth earthquakes in the mantle. *Nature*, *446*(7137), 787–790.

Kennett, B. L. N., & Engdahl, E. R. (1991). Traveltimes for global earthquake location and phase identification. *Geophysical Journal International*, *105*(2), 429–465. http://gji.oxfordjournals.org/content/105/2/429.abstract, https://doi.org/10.1111/j.1365-246X.1991.tb06724.x

Kirby, S. (1995). Interslab earthquakes and phase changes in subducting lithosphere. *Reviews of Geophysics*, *33*(S1), 287–297. https://doi.org/10.1029/95RG00353

Kita, S., & Ferrand, T. P. (2018). Physical mechanisms of oceanic mantle earthquakes: Comparison of natural and experimental events. *Scientific Reports*, *8*(1), 17049. https://doi.org/10.1038/s41598-018-35290-x

Kita, S., Okada, T., Hasegawa, A., Nakajima, J., & Matsuzawa, T. (2010). Existence of interplane earthquakes and neutral stress boundary between the upper and lower planes of the double seismic zone beneath Tohoku and Hokkaido, northeastern Japan. *Tectonophysics*, *496*(1-4), 68–82. http://www.sciencedirect.com/science/article/pii/S0040195110004439, https://doi.org/10.1016/j.tecto.2010.10.010

Korenaga, J. (2017). On the extent of mantle hydration caused by plate bending. *Earth and Planetary Science Letters*, *457*, 1–9.
Lin, G., & Shearer, P. (2005). Tests of relative earthquake location techniques using synthetic data. *Journal of Geophysical Research*, *110*, B04304. https://doi.org/10.1029/2004JB003380
McGuire, J. J., & Wiens, D. A. (1995). A double seismic zone in New Britain and the morphology of the Solomon Plate at intermediate depths. *Geophysical Research Letters*, *22*(15), 1965–1968. https://doi.org/10.1029/95GL01806
Nishikawa, T., & Ide, S. (2014). Earthquake size distribution in subduction zones linked to slab buoyancy. *Nature Geoscience*, *7*(12), 904–908.
Ohuchi, T., Lei, X. L., Ohfuji, H., Higo, Y. J., Tange, Y., Sakai, T., et al. (2017). Intermediate-depth earthquakes linked to localized heating in dunite and harzburgite. *Nature Geoscience*, *10*(10), 771–776. https://doi.org/10.1038/ngeo3011
Okazaki, K., & Hirth, G. (2016). Dehydration of lawsonite could directly trigger earthquakes in subducting oceanic crust. *Nature*, *530*(7588), 81–84. https://doi.org/10.1038/nature16501
Pacheco, J. F., Scholz, C. H., & Sykes, L. R. (1992). Changes in frequency–size relationship from small to large earthquakes. *Nature*, *355*(6355), 71–73. https://doi.org/10.1038/355071a0
Peacock, S. M. (2001). Are the lower planes of double seismic zones caused by serpentine dehydration in subducting oceanic mantle? *Geology*, *29*(4), 299–302. https://doi.org/10.1130/0091-7613(2001)029<0299:ATLPOD>2.0.CO;2
Prieto, G. A., Beroza, G. C., Barrett, S. A., López, G. A., & Florez, M. (2012). Earthquake nests as natural laboratories for the study of intermediate-depth earthquake mechanics. *Tectonophysics*, *570*, 42–56.
Proctor, B., & Hirth, G. (2015). Role of pore fluid pressure on transient strength changes and fabric development during serpentine dehydration at mantle conditions: Implications for subduction-zone seismicity. *Earth and Planetary Science Letters*, *421*, 1–12.
Ranero, C. R., Morgan, J. P., McIntosh, K., & Reichert, C. (2003). Bending-related faulting and mantle serpentinization at the Middle America trench. *Nature*, *425*(6956), 367–373.
Reynard, B., Nakajima, J., & Kawakatsu, H. (2010). Earthquakes and plastic deformation of anhydrous slab mantle in double Wadati-Benioff zones. *Geophysical Research Letters*, *37*, L24309. https://doi.org/10.1029/2010GL045494
Richards-Dinger, K. B., & Shearer, P. M. (2000). Earthquake locations in southern California obtained using source-specific station terms. *Journal of Geophysical Research*, *105*(B5), 10,939–10,960.
Rietbrock, A., & Waldhauser, F. (2004). A narrowly spaced double-seismic zone in the subducting Nazca plate. *Geophysical Research Letters*, *31*, L10608. https://doi.org/10.1029/2004GL019610
Scambelluri, M., Pennacchioni, G., Gilio, M., Bestmann, M., Plümper, O., & Nestola, F. (2017). Fossil intermediate-depth earthquakes in subducting slabs linked to differential stress release. *Nature Geoscience*, *10*(12), 960–966. https://doi.org/10.1038/s41561-017-0010-7
Schlaphorst, D., Kendall, J. M., Collier, J. S., Verdon, J. P., Blundy, J., Baptie, B., et al. (2016). Water, oceanic fracture zones and the lubrication of subducting plate boundaries-insights from seismicity. *Geophysical Journal International*, *204*(3), 1405–1420. https://doi.org/10.1093/gji/ggv509
Schorlemmer, D., Wiemer, S., & Wyss, M. (2005). Variations in earthquake-size distribution across different stress regimes. *Nature*, *437*(7058), 539.
Shearer, P. M. (1997). Improving local earthquake locations using the L1 norm and waveform cross correlation: Application to the Whittier Narrows, California, aftershock sequence. *Journal of Geophysical Research*, *102*(B4), 8269–8283.
Syracuse, E. M., Abers, G. A., Fischer, K., MacKenzie, L., Rychert, C., Protti, M., et al. (2008). Seismic tomography and earthquake locations in the Nicaraguan and Costa Rican upper mantle. *Geochemistry, Geophysics, Geosystems*, *9*, Q07S08. https://doi.org/10.1029/2008GC001963
Syracuse, E. M., van Keken, P. E., & Abers, G. A. (2010). The global range of subduction zone thermal models. *Physics of the Earth and Planetary Interiors*, *183*(1-2), 73–90. http://www.sciencedirect.com/science/article/pii/S0031920110000300, https://doi.org/10.1016/j.pepi.2010.02.004
van Stiphout, T., Kissling, E., Wiemer, S., & Ruppert, N. (2009). Magmatic processes in the Alaska subduction zone by combined 3-D b value imaging and targeted seismic tomography. *Journal of Geophysical Research*, *114*, B11302. https://doi.org/10.1029/2008JB005958
Waldhauser, F., & Ellsworth, W. L. (2000). A double-difference earthquake location algorithm: Method and application to the northern Hayward fault, California. *Bulletin of the Seismological Society of America*, *90*(6), 1353–1368. http://www.bssaonline.org/content/90/6/1353.abstract, https://doi.org/10.1785/0120000006
Wei, S. S., Wiens, D. A., van Keken, P. E., & Cai, C. (2017). Slab temperature controls on the Tonga double seismic zone and slab mantle dehydration. *Science Advances*, *3*(1), e1601755. https://doi.org/10.1126/sciadv.1601755
Wiemer, S., & Benoit, J. P. (1996). Mapping the B-value anomaly at 100 km depth in the Alaska and New Zealand Subduction Zones. *Geophysical Research Letters*, *23*(13), 1557–1560. https://doi.org/10.1029/96GL01233
Wiemer, S., & Wyss, M. (2000). Minimum magnitude of completeness in earthquake catalogs: Examples from Alaska, the western United States, and Japan. *Bulletin of the Seismological Society of America*, *90*(4), 859–869.
Wiens, D. (2001). Seismological constraints on the mechanism of deep earthquakes: Temperature of deep earthquake source properties. *Physics of the Earth and Planetary Interiors*, *127*, 145–163.
Woessner, J., & Wiemer, S. (2005). Assessing the quality of earthquake catalogues: Estimating the magnitude of completeness and its uncertainty. *Bulletin of the Seismological Society of America*, *95*(2), 684–698.
Wyss, M., Hasegawa, A., & Nakajima, J. (2001). Source and path of magma for volcanoes in the subduction zone of northeastern Japan. *Geophysical Research Letters*, *28*(9), 1819–1822. https://doi.org/10.1029/2000GL012558
Yamasaki, T., & Seno, T. (2003). Double seismic zone and dehydration embrittlement of the subducting slab. *Journal of Geophysical Research*, *108*(B4), 2212. https://doi.org/10.1029/2002JB001918
Zhang, H. J., Thurber, C. H., Shelly, D., Ide, S., Beroza, G. C., & Hasegawa, A. (2004). High-resolution subducting-slab structure beneath northern Honshu, Japan, revealed by double-difference tomography. *Geology*, *32*(4), 361–364.

References From the Supporting Information

Ekstrom, G., Nettles, M., & Dziewonski, A. M. (2012). The global CMT project 2004-2010: Centroid-moment tensors for 13,017 earthquakes. *Physics of the Earth and Planetary Interiors*, *200*, 1–9.
International Seismological Centre (2018). ISC-EHB bulletin. *Internatl. Seismol. Cent*.
Paternoster, R., Brame, R., Mazerolle, P., & Piquero, A. (1998). Using the correct statistical test for the equality of regression coefficients. *Criminology*, *36*(4), 859–866. https://doi.org/10.1111/j.1745-9125.1998.tb01268.x